Ni(^{1}O, ^{12}C) ^{2}Zn Reaction at an Incident Energy 80 MeV

AUTHOR(S):

Ōkuma, Yasuhiko; Motobayashi, Tooru; Takimoto, Kiyohiko; Shimoura, Susumu; Ogino, Kouya; Fukada, Mamoru; Suehiro, Teruo; Matsuki, Seishi; Yanabu, Takuji

CITATION:

Ōkuma, Yasuhiko ...[et al]. Ni(^{1}O, ^{12}C) ^{2}Zn Reaction at an Incident Energy 80 MeV. Bulletin of the Institute for Chemical Research, Kyoto University 1983, 61(1): 12-29

ISSUE DATE:

1983-03-25

URL:

http://hdl.handle.net/2433/77018

Bull. Inst. Chem. Res., Kyoto Univ., Vol. 61, No. 1, 1983

^{58}Ni(^{16}O, ^{12}C) ^{62}Zn Reaction at an Incident Energy 80 MeV*

Yasuhiko ŌKUMA, Tooru MOTOBAYASHI*, Kiyohiko TAKIMOTO**,
Susumu SHIMOURA**, Kouya OGINO***, Mamoru FUKADA†,
Teruo SUEHIRO††, Seishi MATSUKI††† and Takuji YANABU†††

Received January 18, 1983

Cross section angular distributions for the ^{16}O+^{58}Ni elastic scattering and the ^{58}Ni(^{16}O, ^{12}C)^{62}Zn–3.8416 MeV reaction leading to the discrete and continuum states at an incident energy E_{lab}(^{16}O) =80 MeV have been measured. The eight low-lying single and double energy levels were observed in the energy spectra of the ^{58}Ni(^{16}O, ^{12}C)^{62}Zn reaction. Populations of these levels have the cross sections of 1–200 μb/sr. The total yield of the (^{16}O, ^{12}C) reaction was enhanced in the particle-identification spectra of the ^{16}O induced reactions on ^{58}Ni. This is because the Q value of this reaction is negative but small. The g'nd state cross section was proved to change with the incident energy by comparing the present data with the other 46 and 60 MeV data. The cross section angular distribution for the g'nd state transition changes also with the incident energy. The data points for the 46 MeV incident energy show a typical bell shape angular distribution. The angular distribution for the 60 MeV incident energy reveals a forward peaked and pronounced oscillation pattern, while that for the 80 MeV incident energy shows an oscillation damping with the angle and then a monotonous fall on the angle. Optical model parameters were deduced from the best fit to the measurements of the ^{16}O+^{58}Ni elastic scattering. The EFR-DWBA calculations of the (^{16}O, ^{12}C) results were performed with reasonable fits for the cross section angular distributions of observed energy levels. The optical model parameters giving good representations of the α-transfer data have the property that the real diffuseness parameter has a large value almost equal to the radius parameter. The inclusion of Coulomb correction in the transfer interaction causes a reduction of 0.9 times in cross section, but no change in angular distribution. The dependence of the angular distribution shape on the incident energy can be reproduced by the EFR-DWBA calculation even if only one parameter set is used in the calculation over the wide incident energy range. Relative spectroscopic factors were deduced from comparison of data with calculations. The deduced factors are in reasonable agreement with results of the other (^{16}O, ^{12}C), (^{12}C, ^{8}Be) and (^{6}Li, d) reactions, and of the shell model calculations. The reaction coefficients are consistent with those at 46 and 60 MeV.

KEY WORDS : Nuclear reaction ^{58}Ni(^{16}O, ^{12}C)^{62}Zn E=80 MeV ;
measured σ(E, θ)/ Reaction mechanism/ EFR-DWBA calculation/

§1. INTRODUCTION

Extensive investigations of multinucleon transfer reactions induced by heavy ions

* This paper is dedicated to Prof. emeritus Takuji Yanabu.

大隈靖彦 Research Center for Nuclear Physics, Osaka University, Ibaraki, Osaka,
* 本林 透 Department of Physics, Faculty of Science, Osaka University, Toyonaka, Osaka
** 滝本清彦, 下浦 亨 Department of Physics, Faculty of Science, Kyoto University, Kyoto
*** 荻野晃也 Department of Nuclear Engineering, Faculty of Engineering, Kyoto Univeristy, Kyoto
† 深田 守 Department of Physics, Kyoto College of Pharmacy, Kyoto
†† 末広輝男 Department of Physics, Tohoku Institute of Technology, Sendai, Miyagi
††† 松木征史, 柳父琢治 Keage Laboratory, Institute for Chemical Research, Kyoto University, Kyoto

have been done experimentally as well as theoretically. Those have been studied to identify the multiparticle-multihole states in nuclei and obtain informations on their nuclear structures by comparing different reactions reaching the same residual nucleus. The studies of the four nucleon correlations in nuclei, particularly at the nuclear surface, are one of the most interesting aspects of multinucleon transfer reactions.

The lithium-induced reactions are the best processes to examine α clustering in nuclei from the considerations of spectroscopic factors.[1] The (^{6}Li, d) or (^{7}Li, t) stripping reactions have been devoted to the study of multiparticle-multihole configurations in $N=Z$ even light nuclei and four particle-four hole (4p−4h) deformed configurations have been identified as the main contributors to the rotational bands observed in ^{16}O and ^{40}Ca.[2] Since it was found that the cross sections of (^{6}Li, d) or (^{7}Li, t) reactions were drasticaly decreasing functions of mass number, the (^{16}O, ^{12}C) stripping reaction became to be used as an alternative to the lithium-induced reactions. The selectivity of these (^{16}O, ^{12}C) and (^{6}Li, d) reactions to individual transitions appears to be very similar.[3,4] Whether the four nucleons transferred in the (^{16}O, ^{12}C) reaction behave like an α particle has been much discussed.[3~7] Despite several studies the mechanism of the (^{16}O, ^{12}C) reaction has not yet been well understood.[8,9]

In single closed shell nuclei, a few results based mostly on the discussion of spin sequences in the framework of collective model suggest the existence of quasirotational bands.[10,11] It has been attempted to look for excited states in the quasirotational bands by a direct α transfer reaction.[12,14] It has been suggested that the observed strong selectivity in the population of the final states in the (^{16}O, ^{12}C) reaction on 1f−2p shell target nuclei might reveal a quartet structure of nuclei. Also, the existence of α vibrational states, that are excited by the α transfer reactions such as (^{6}Li, d), (^{16}O, ^{12}C), etc., was predicted from the proton and neutron pairing vibrational states excited by the two-nucleon transfer reactions.[15] The pairing-vibration model was extended to include α transfer reactions and compared with experimental results, particularly $J^\pi=0^+$ states for medium nuclei.[16,17] However, no reliable nuclear structure information could be obtained, because not enough was known about the reaction mechanism of the (^{16}O, ^{12}C) reaction.

The cross section angular distributions of the discrete and continuum states in the ^{62}Zn populated by the ^{58}Ni(^{16}O, ^{12}C)^{62}Zn−3.8416 MeV reaction at an incident energy $E_{lab}(^{16}O)=80$ MeV were measured by ordinary $\Delta E-E$ solid state detector telescopes. The aim of the present investigation is to obtain informations on the reaction mechanism of the (^{16}O, ^{12}C) reaction and on the four nucleon correlations at the nuclear surface in medium weight nuclei. The measured ^{58}Ni(^{16}O, ^{12}C)^{62}Zn transitions were compared with the results of the exact finite range distorted wave Born approximation (EFR-DWBA) calculations. The ^{16}O+^{58}Ni elastic scattering angular distribution was measured at the same incident energy as the transfer reaction in order to determine optical model (OM) parameters necessary for the EFR-DWBA calculations and to normalize transfer reaction data. Part of the present work was reported already elsewhere.[18~20]

This paper describes the experimental method and procedure in Sect. 2, the experimental results in Sect. 3, the OM calculation for the elastic scattering and the EFR-DWBA calculation for the transfer reaction in Sect. 4, and the analyses and discussions of

the experimental and calculated results in Sect. 5.

§ 2. EXPERIMENTAL METHOD AND PROCEDURE

The experiments were carried out at the RCNP-AVF cyclotron using an oxygen-16 beam in the 4^+ charge state at 80 MeV. Angular distributions were measured in a 100 cm diameter scattering chamber maintained at a vacuum of better than 2×10^{-5} Torr and essentially free from organic contaminants. The beam current measured with a Faraday cup was below 50 enA. The reaction products were detected by two standard ΔE-E counter telescopes. Highly enriched metallic self-supporting nickel-58 targets were of 485.2 and 473 μg/cm^2 thickness.

The reaction products were identified by the standard ΔE−E counter telescope, each of them consisting of a thin ΔE (30 μm) and a thicker E(300 μm) ORTEC silicon semiconductor surface barrier detectors. The secondary electrons from the target affect the resolution of the detectors, so that a weak magnetic field ($\sim$300 G) was applied in front of the detectors and a 1 kV positive bias was applied to the target. The over-all resolution of 6×10^{-3} was obtained for the elastic scattering data. A monitor E solid state detector mounted at 14.7° served to normalize the data.

The fast-slow coincidence circuit with an elastic scattering rejection subcircuit of the ΔE-E counter telescope was made up by the ORTEC-NIM modules. The schematic diagram of the electronics is presented in Fig. 1. The signals from elastically scattered ^{16}O ions were cut-off by means of the single-channel analyzers to avoid overloading of the computer. After the amplification, gating, shaping and analog-to-digital conversion, the ΔE and E signals were sent to a RAW DATA PROCESSOR. The digitized raw data of the ΔE and E were analyzed on line with a PDP 11/40 computer and at the same time written event-by-event on a magnetic tape for subsequent detailed analyses

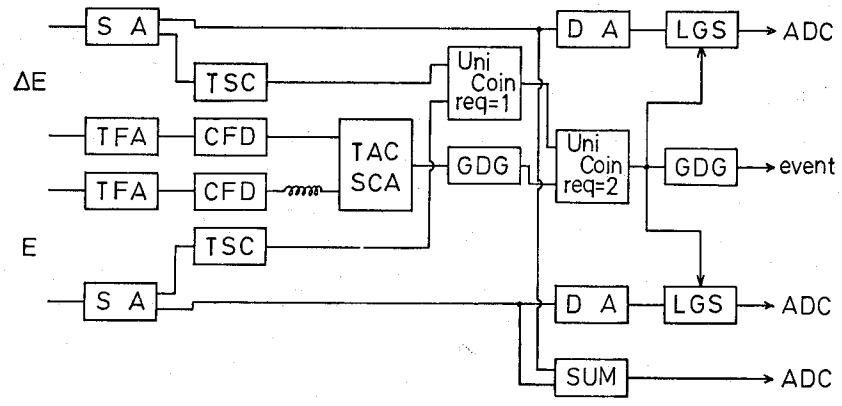

Fig. 1, Schematic block diagram of the ΔE-E counter telescope electronics. SA: Spectrojcopy amp., DA: delay amp., LGS: linear gate and strecher, TSC: timing single channel, TFA: timing filter amp., CFD: constant fraction discriminator, TACSCA: time to pulse height converter/SCA, Univ Coin: universal coincidence, GDG: gate and delay generator, SUM: dual sum and invert amp., ADC: analog-to-digital convertor and event: event signal for RAW DATA PROCESSOR.

with a TOSBAC 5600 computer. Also, a ($\Delta E+E$) gate free signal was analyzed by a multichannel pulse height analyzer to store the elastic scattering data.

The oxygen, nitorogen and carbon isotopes were well separated. Thus, the cross sections for different reactions can be directly compared. All yields were corrected for the electronics dead time and normalized to the elastic scattering data. Absolute cross sections were estimated to be accurate within 15%. This uncertainty resulted from the deviation of the measured elastic scattering from the calculated Rutherford cross section, the uncertainty in the ratio of solid angles in two counters and the uncertainty in the ratio of experiments in two data taking times.

§3. EXPERIMENTAL RESULTS

3-1. Elastic Scattering

The $^{16}O+^{58}Ni$ elastic scattering at the incident energy $E_{lab}(^{16}O)=80$ MeV was measured to provide OM parameters necessary to calculate the distorted wave of the entrance channel in the EFR-DWBA calculations and to normalize the α transfer reaction yields.

Figure 2 shows an energy spectrum of the $^{16}O+^{58}Ni$ elastic and inelastic scatterings at the incident energy $E_{lab}(^{16}O)=80$ MeV and at a detection angle $\theta_{lab}(^{16}O)=34.75°$. The obtained resolution allowed to separate several peaks from the large tail of the

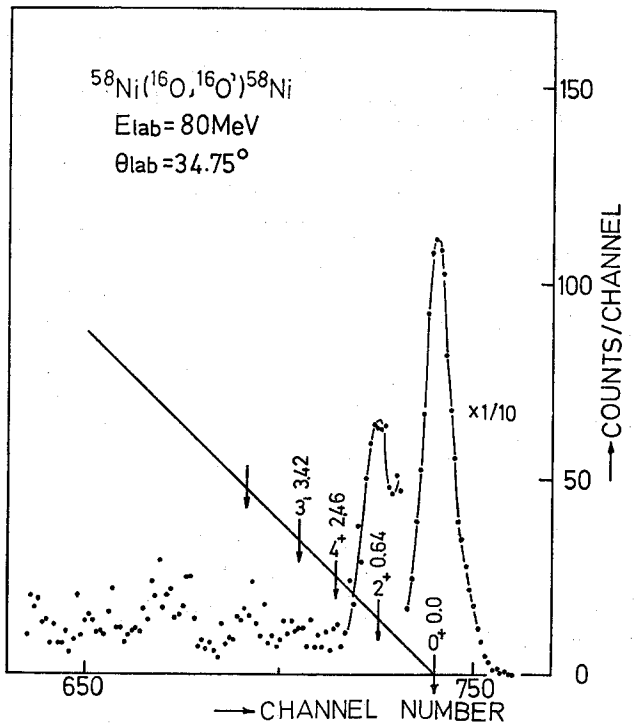

Fig. 2, Energy spectrum of the $^{16}O+^{58}Ni$ scattering at the incident energy $E_{lab}(^{16}O)=80$ MeV and the measured angle $\theta_{lab}(^{16}O)=34.75°$.

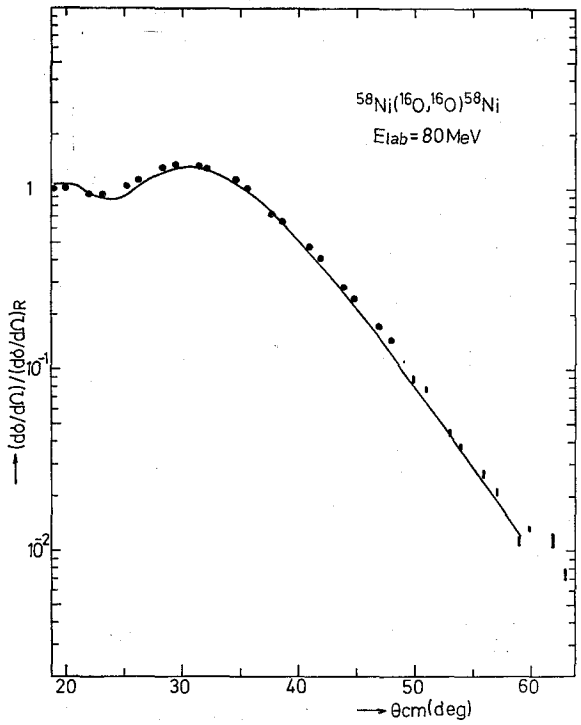

Fig. 3, Measured cross ssection angular distribution of the $^{16}O+^{58}Ni$ elastic scattering at the incident energy $E_{lab}(^{16}O)=80$ MeV represented as the ratio to the Rutherford cross section. A curve shows the calculation using the OM potential described in the text. Error bars indicate only the statistical ones.

elastic peak, one of which can be identified as the 1.45 MeV 2^+ state by comparison with other scattering and reaction measurements.[21] Fig. 3 presents an angular distribution of the $^{16}O+^{58}Ni$ elastic scattering at the incident energy $E_{lab}(^{16}O)=80$ MeV represented as the ratio to the Rutherford cross section. In order to determine the normalization factor for the absolute cross section, it was assumed for the $^{16}O+^{58}Ni$ elastic scattering to be pure Rutherford scattering at measured smallest angles $\theta_{lab}(^{16}O)=14.75°$ and 15.63°. All cross sections were normalized to the calculated Rutherford cross sections at these scattering angles. Error bars indicate only statistical ones. A curve in data points represents the OM calculation which is described in sect. 4-1.

3-2. Transfer Reaction

A typical overall energy spectrum of the $^{58}Ni(^{16}O, ^{12}C)^{62}Zn$ reaction at the incident energy $E_{lab}(^{16}O)=80$ MeV and at the measured angle $\theta_{lab}(^{12}C)=19.75°$ is shown in Fig. 4. This energy spectrum shows a broad peak at the excitation energy of around 16 MeV.

Figures 5 and 6 show the low excitation energy parts of the energy spectra of the $^{58}Ni(^{16}O, ^{12}C)^{62}Zn$ reaction at the incident energy $E_{lab}(^{16}O)=80$ MeV, and at the measured angles $\theta_{lab}(^{12}C)=19.75°$ and 34.75°, respectively. Several groups of states are

seen in both angles. The g'nd state and several low-lying levels were weakly populated. The resolution obtained with the present ^{58}Ni target and ^{16}O beam allowed to identify some low-lying energy levels including overlapping levels in the ^{62}Zn residual nucleus by comparison with other scattering and reaction measurements.[21] The energy levels were

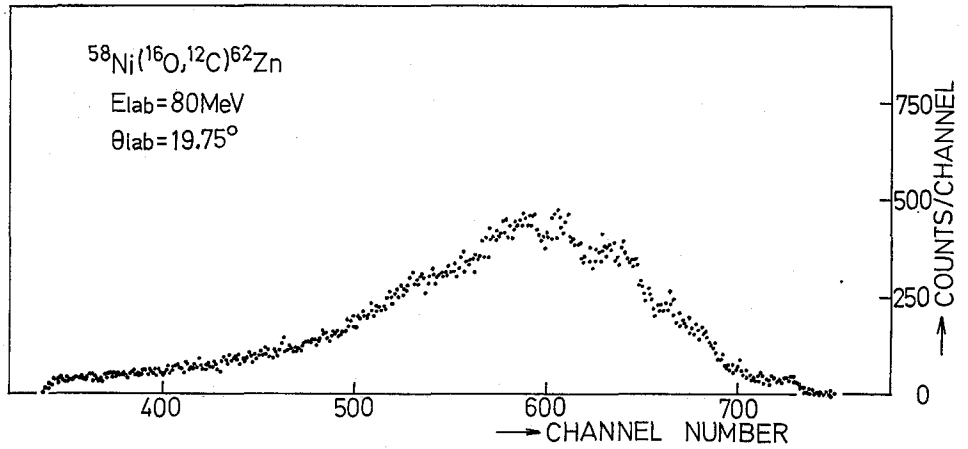

Fig. 4, Continuum energy spectrum of the $^{58}Ni(^{16}O, ^{12}C)^{62}Zn$ reaction at the incident energy $E_{lab}(^{16}O) = 80$ MeV and the measured angle $\theta_{lab}(^{12}C) = 19.75°$.

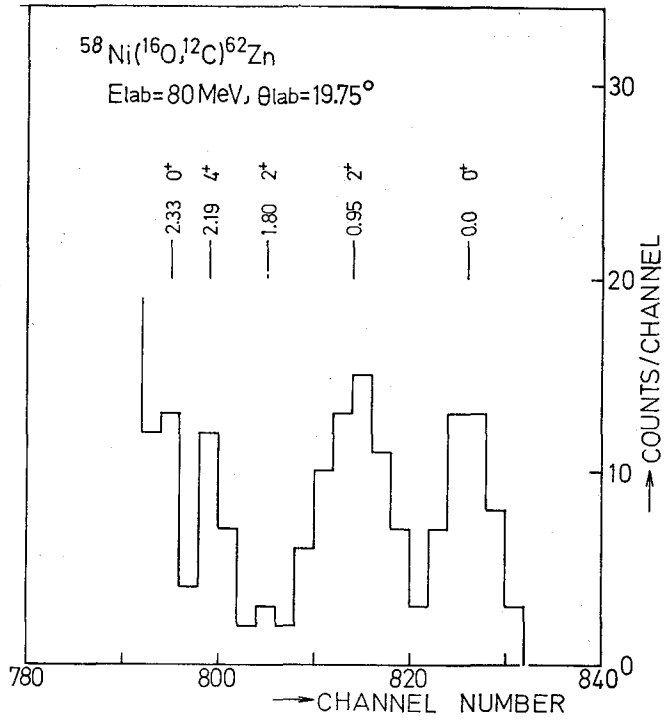

Fig. 5, Energy spectrum of the $^{58}Ni(^{16}O, ^{12}C)^{62}Zn$ reaction at the incident energy $E_{lab}(^{16}O) = 80$ MeV and the measured angle $\theta_{lab}(^{12}C) = 19.75°$.

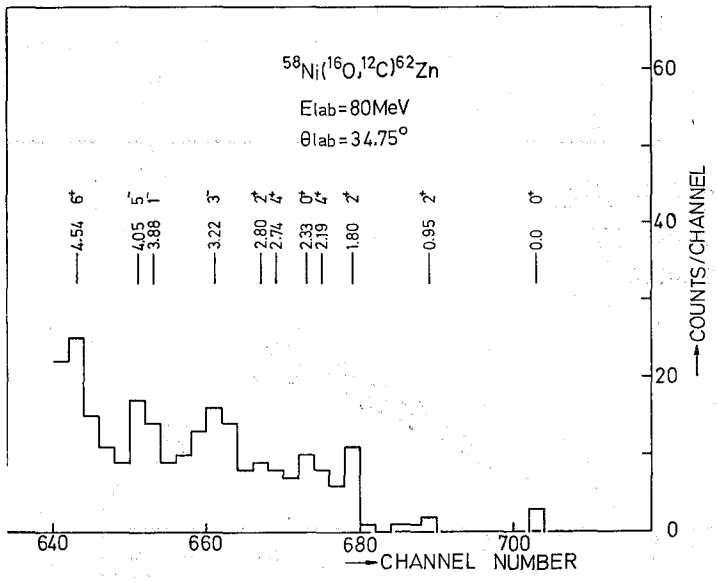

Fig. 6, Energy spectrum of the $^{58}Ni(^{16}O, ^{12}C)^{62}Zn$ reaction at the incident energy $E_{lab}(^{16}O) = 80$ MeV and the measured angle $\theta_{lab}(^{12}C) = 34.75°$.

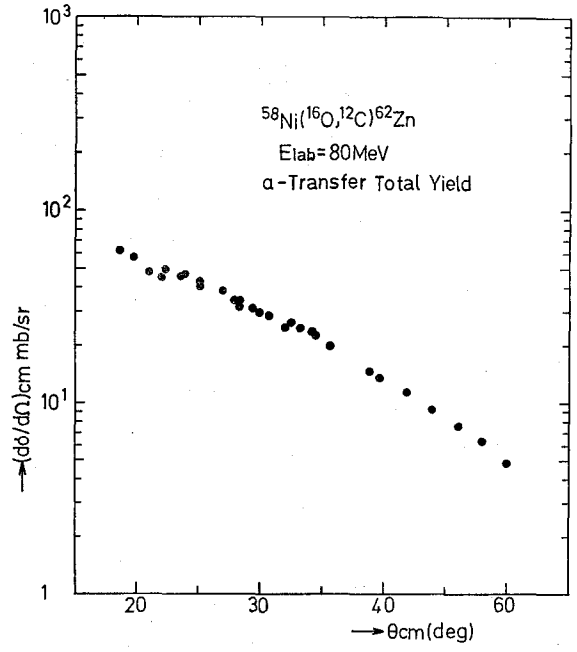

Fig. 7, Measured cross section angular distribution of the $^{58}Ni(^{16}O, ^{12}C)^{62}Zn$ reaction at the incident energy $E_{lab}(^{16}O) = 80$ MeV leading to the continuum state in the ^{62}Zn.

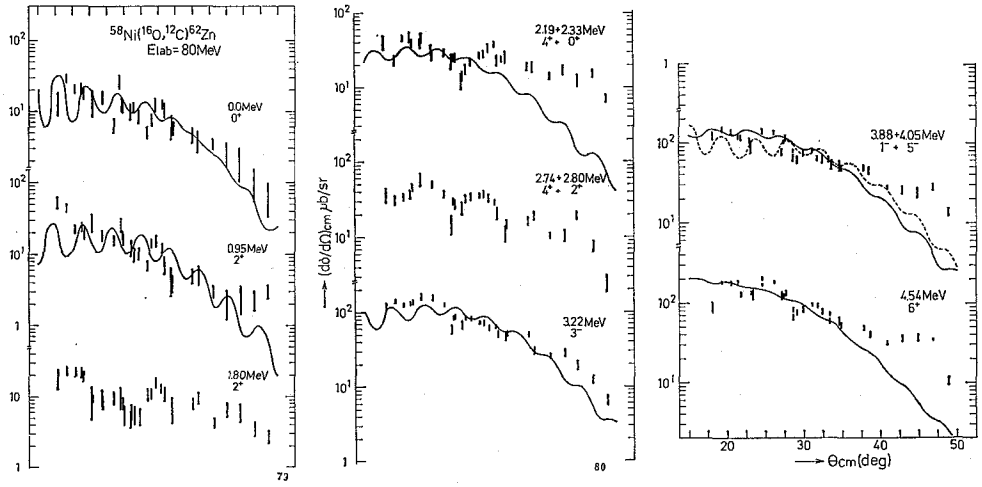

Fig. 8, Measured cross section angular distributions of the ^{58}Ni(^{16}O, ^{12}C)^{62}Zn reaction at the incident energy E_{lab}(^{16}O) = 80 MeV leading to the low-lying states, 0.0 MeV 0^+, 0.95 MeV 2^+, 1.81 MeV 2^+, 2.19 MeV 4^++2.33 MeV 0^+, 2.74 MeV 4^++2.80 MeV 2^+, 3.22 MeV 3^-, 3.88 MeV 1^-+4.05 MeV 5^- and 4.54 MeV 6^+ in the ^{62}Zn. The experimental results are compared with the EFR-DWBA predictions. For the 2.19+2.33 MeV transitions, only the prediction for the 2.19 MeV, 4^+ state is shown as solid line. Also, only the 3.88 MeV 1^- state, and only the 4.50 MeV 5^- state were taken into account in the predictions as dotted and solid lines, respectively. Error bars indicate only statistical.

adopted only if their peaks were seen at least in three different angles. These energy levels are indicated in Figs. 5 and 6. These excitation energies E_x are listed in Table 2.

Figure 7 shows a measured cross section angular distribution of the ^{58}Ni(^{16}O, ^{12}C) ^{62}Zn reaction leading to the continuum state in the ^{62}Zn residual nucleus.

The measured cross section angular distributions of the ^{58}Ni(^{16}O, ^{12}C)^{62}Zn reaction leading to the discrete states in the ^{62}Zn residual nucleus are presented in Fig. 8. The data were taken in the angular range θ_{lab}(^{12}C) = 14.5° − 39.75° in $\Delta\theta_{lab}$(^{12}C) = 1° or 1.25° steps in order to resolve the oscillations for the 0^+ and 2^+ transitions which are discussed in sect. 5-2. The g'nd state angular distribution exhibits an oscillation damping with the reaction angle and then a monotonous fall on the reaction angle.

§ 4. CALCULATIONS

4-1. Optical model calculation

The EFR-DWBA analysis of the ^{58}Ni(^{16}O, ^{12}C)^{62}Zn reaction requires the knowledge of the wave functions which describe the elastic scatterings in the entrance and exit channels. To provide the OM parameters necessary to calculate the entrance channel wave function, the ^{16}O+^{58}Ni elastic scattering data were refitted by using the OM starting parameters from the literature.[22] The calculation was performed by using a potential with a Woods-Saxon form factor for both the real and imaginary parts. The potential depth, radius and diffuseness parameters are denoted V, r_R, a_R, and W, r_I, a_I

Table I, Optical model parameters used in the present calculations. The Coulomb radius r_c is 1.25 fm for all potentials.

		V(MeV)	r_R (fm)	a_R (fm)	W(MeV)	r_W (fm)	a_W (fm)
I	a) Starting parameters to* elastic scattering data	−70.	1.18	0.57	−82.1	1.18	0.39
	b) Fitting parameters to elastic scattering data	−70.	1.121	0.57	−82.	1.121	0.39
	c) Parameters used in EFR-DWBA calculations	−70.	1.18	1.026	−82.	1.18	0.39
II	$E_{lab}(^{16}O)$=80 MeV	−70.	1.18	1.026	−82.	1.18	0.39
	=60 MeV**	−45.09	1.298	0.461	−57.39	1.217	0.163
	=46 MeV**	−40.74	1.303	0.473	−59.19	1.216	0.164

*; Ref. 22, **; Ref. 8

for the real and the imaginary potentials, respectively. The potential radius is defined as $R=r(A_a^{1/3}+A_A^{1/3})$ for both potentials where A_a and A_A are the mass numbers of projectile and target. The radius parameter of the Coulomb potential $r_c=1.25$ fm was fixed for all calculations. All six parameters were allowed to vary to obtain the best fits. Table 1 gives the starting parameters and the best fitted parameters. The OM fitting results to the $^{16}O+^{85}Ni$ elastic scattering data points is represented by a solid curve in Fig. 2.

4-2. Exact finite range distorted wave Born approximation calculation

The measured cross section angular distributions of the $^{58}Ni(^{16}O, ^{12}C)^{62}Zn$ reaction were analyzed by the exact finite range distorted wave Born approximation (EFR-DWBA) employing the computer code LOLA of DeVries.[23]

The two proton-two neutron transfer was treated in the cluster approximation or in the simple model assuming that the reaction proceeds by a one-step direct transfer process. The transferred particles were considered to be an α cluster in its 0s ground state. Under these assumptions, the experimental cross section for a stripping reaction $A(a, b)B$, $B=A+\alpha$ and $a=b+\alpha$, where A, B, a, b and α represent the target nucleus, residual nucleus, incident particle, outgoing particle and transferred α cluster, can be written as

$$\frac{d\sigma}{d\Omega}\Big)^{l}_{exp} = R\cdot S_{ab}S_{AB}\cdot\frac{d\sigma}{d\Omega}\Big)^{l}_{DWBA} \qquad (1)$$

where $d\sigma/d\Omega)^{l}_{DWBA}$ is the calculated cross section, S_{ab} and S_{AB} denote the spectroscopic factors for the light system ab ($a=^{16}O$, $b=^{12}C$) and the heavy system AB ($A=^{58}Ni$, $B=^{62}Zn$), respectively, and R is the reaction coefficient. The factors $S_{ab}S_{AB}$ are to be determined from Eq. (1) by comparing experimental and theoretical cross sections. However, the reaction coefficient R has been introduced because the DWBA calculations for heavy ion reactions are generally unable to reproduce absolute cross sections. Only relative spectroscopic factors or ratios of the excited state spectroscopic factor to the g'nd state spectroscopic factor $S_{ab}S_{AB}/(S_{ab}S_{AB})_{g.s.}$ were thus considered in the following analyses.

Woods-Saxon potentials were used to calculate bound state wave functions. The

potential radius is defined as $R=r(A_a^{1/3}+A_{A\text{ or }b}^{1/3})$ where A_a and $A_{A\text{ or }b}$ are the mass numbers of the transferred α cluster and the target nucleus or outgoing particle, respectively. The potential geometry was fixed to a radius parameter of $r=1.25$ fm and a diffuseness parameter of $a=0.65$ fm. The potential depth was adjusted to reproduce the experimental binding energy of the α cluster in the system $^{58}Ni+\alpha$ or $^{12}C+\alpha$. The number of nodes N and the orbital angular momentum L for the bound state wave functions follow the Talmi-Moshinsky relationship:[24]

$$2N+L=\sum_{i=1}^{4}(2n_i+l_i), \qquad (2)$$

where n_i and l_i are the number of nodes and orbital angular momentum of harmonic oscillator states of the ^{58}Ni and ^{12}C cores into which the four nucleons transfer. In case the target has spin zero, as in this experiment, the orbital angular momentum L of the bound α is equal to the spin of the residual nucleus J, and parity $\pi=(-1)^L$, i. e., normal parity. To calculate the number of nodes, particular configurations of the four nucleons in the projectile ^{16}O and in the final state ^{62}Zn have to be assumed. The configuration taken for the system $^{16}O=^{12}C+\alpha$ is $N=2$ and $L=0$. The configurations N and L, and spins-parities J^π assumed for the system $^{62}Zn=^{58}Ni+\alpha$ are listed in Table 2. It has been shown by DeVries[25] that in the EFR-DWBA calculations of multinucleon transfer reactions the inclusion of the Coulomb correction in the transfer interaction makes the deviation of less than 20% in magnitude.

The starting OM parameters were determined by fitting the experimental cross section angular distribution of the $^{16}O+^{58}Ni$ elastic scattering. Since no OM parameters for the exit channel are available, the same potential parameters were used in exit and entrance channels. All six parameters in the entrance and exit channels were allowed to vary to obtain the best fits. The OM parameter set I used in the EFR-DWBA calculations is listed in Table I.

The EFR-DWBA fitting results to the $^{56}Ni(^{16}O, ^{12}C)^{62}Zn$ reaction data points are represented by curves in Fig. 8.

§ 5. ANALYSES AND DISCUSSIONS

5-1. Energy levels and their cross sections

The energy levels observed in the $^{58}Ni(^{16}O, ^{12}C)^{62}Zn$ reaction are summarized in Table 2. These are shown together with the results from other $(^{16}O, ^{12}C)$[8,12], $(^{12}C, ^{8}Be)$[26], $(^{6}Li, d)$[27,28,16], (τ, n)[24,30] and (p, t)[31] reactions in Fig. 9. The 0.0 MeV 0^+ g'nd state, 0.95 MeV 2^+ l'st excited state and 3.22 MeV 3^- state were observed in all quoted reactions. These levels have the cross sections of 1-200 μb/sr. The selectivity of the $(^{16}O, ^{12}C)$ reaction appears to be similar to the $(^{6}Li, d)$ reaction. Such similarities have also been observed by comparison between the $(^{16}O, ^{12}C)$ and $(^{6}Li, d)$ reactions on ^{40}Ca,[3] ^{24}Mg and ^{28}Si,[32] and $^{54,56,58}Fe$[4] nuclei.

The energy levels of ^{62}Zn are compared with the shell model predictions of Bennett et al,[33] which included $2p_{3/2}$, $1f_{3/2}$ and $2p_{1/2}$ orbitals outside an innert ^{58}Ni core in Fig. 10. The calculated excitation energies appear to provide good fits to the observed

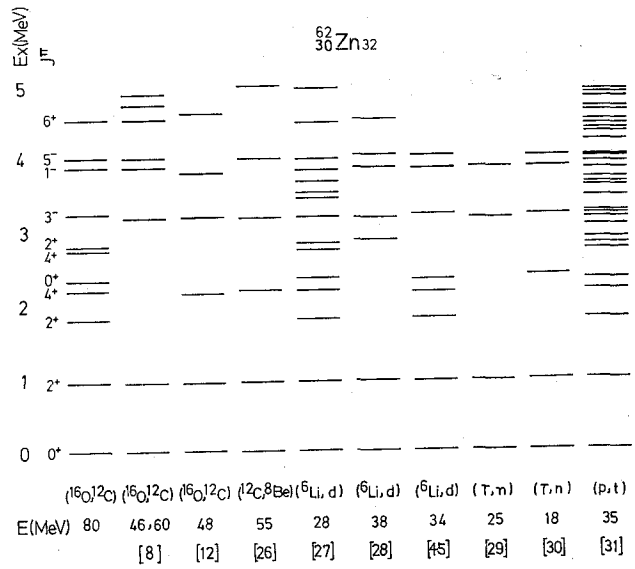

Fig. 9. Energy levels in ^{62}Zn in this experiment and those in the other (^{16}O, ^{12}C), (^{12}C, ^{8}Be), (^{6}Li, d), (τ, n) and (p, t) reactions. Numbers in parentheses denote reference numbers.

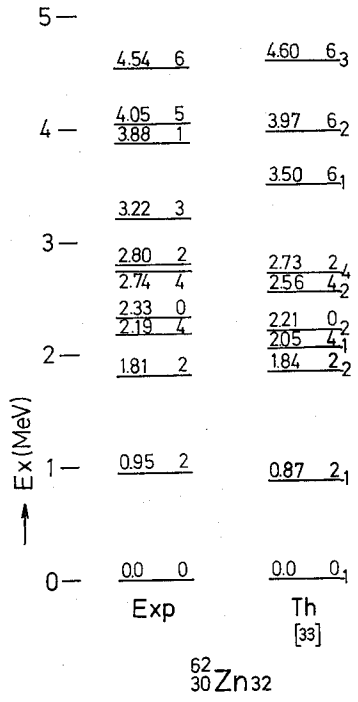

Fig. 10. Energy levels of ^{62}Zn. The levels observed in experiment are shown in the left. They are compared with the calculated energies and spins predicted by Bennett et al.

excitation energies except for 6^+ excitation energies.

The (^{16}O, ^{12}C) reaction cross sections were enhanced in the particle identification spectra. This is because the Q-value for this reaction is negative but small (−3.8416 MeV). It is clear from the comparisons with the other experiments at different energies[8] that the g'nd state cross section changes with the incident energy as shown in Fig. 11.

5-2. Exact finite range distorted wave Born approximation analyses

Results of the EFR-DWBA calculations of cross section angular distributions for the $^{58}Ni(^{16}O, ^{12}C)^{62}Zn$ reaction leading to the g'nd 0.0 MeV 0^+, 0.95 MeV 2^+, 2.19 MeV 4^+, 3.22 MeV 3^-, 3.88 MeV 1^- (dotted curve), 4.05 MeV 5^- and 4.54 MeV 6^+ states are shown in Fig. 8 together with experimental results already presented in sect. 3-2.

The calculations reproduces the overall features of the angular distributions. The experimental and theoretical angular distributions of the 0.0 MeV 0^+ g'nd state show the oscillations damping with the reaction angle and then the smooth decrement on the reaction angle. Those of the 0.95 MeV 2^+ l'st excited state reveal the strong oscillations over the whole angular range. The OM parameters giving a good representation of the transfer data differ by five percents in the radius parameter with those deduced from the fit of the elastic scattering data in Tabel I. Also, it is noted that the real diffuseness parameter is considerably large as shown in Table I. Thus, the present calculations were performed with the OM parameters which do not describe the elastic scattering data. This may be due to the facts that the elastic scattering and transfer reaction are

Table II, The excitation energy E_x, spin-parity J^π, number of nodes N and orbital angular momentum L for the bound state $^{62}Zn = ^{58}Ni + \alpha$, and relative spectroscopic facfor $S_{ab}S_{AB}/(S_{ab}S_{AB})_{g.s.}$ deduced from various α-transfer reactions and theoretical prediction.

Ex (MeV)	J^π	N	L	(^{16}O, ^{12}C) 80 MeV	[8, 36] (^{16}O, ^{12}C)		[26] (^{12}C, ^{8}Be)	[27] (^{6}Li, d) 28 MeV		[28] (^{6}Li, d)	[45] (^{6}Li, d)	[1, 37] Theory
					46 MeV	60 MeV	55 MeV	SBF	III	38 MeV	34 MeV	
				1	1	1	1	1	1	1	1	1
0.00	0	6	0	$(2.0\times10^{-2})^a$	$(8.5\times10^{-3})^a$	$(1.5\times10^{-2})^a$		(0.2)[b]	(0.15)[b]			$(3\times10^{-3})^c$
0.95	2^+	5	2	0.21	0.42	0.40	0.35	0.36	0.29	0.21	0.23	0.56
1.81	2^+							0.016	0.015		0.004	0.0035
2.19	4^+	4	4	0.13				0.055	0.043		0.04	0.069
2.33	0^+							0.12	0.093		0.10	0.0015
2.74	4^+											
2.80	2^+											
3.22	3^-	5	3	0.70	0.38	0.55		0.39	0.037	0.41	0.27	
3.88	1^-	6	1	0.55				0.43	0.48		0.30	
4.05	5^-	4	5	0.19							0.10	
4.54	6^+	3	6	0.22				0.20	0.23			

a; $RS_{ab}S_{AB}$, b; $d\sigma_{exp}/d\Omega_{DWBA}$, c; $S_{ab}S_{AB}$

sensitive to different regions of the OM potential[34,35] and/or simply, the same OM parameters were used in both the entrance and exit channels. The inclusion of the Coulomb correction in the transfer interaction causes reduction of 0.9 times in cross section, but no change in angular distribution.

The factors $R \cdot S_{ab}S_{AB}$ containing the spectroscopic factors were deduced according to Eq. (1) by comparing experimental with theoretical cross sections. In Table II the spectroscopic factors relative to the g'nd state $S_{ab}S_{AB}/(S_{ab}S_{AB})_{g.s.}$ are listed together with results of the other (^{16}O, ^{12}C)[8], (^{12}C, ^{8}Be)[26] and (^{6}Li, d)[10,27,28] reactions. The theoretical spectroscopic factors for the low-lying states shown in Table 2 were obtained from shell model calculations of S_{ab} for the (^{16}O-^{12}C) system[1] and S_{AB} for the (^{58}Ni-^{62}Zn) system.[37] The absolute spectroscopic factors of the g'nd state transition are given in parentheses when known. Relative spectroscopic factors from different α transfer reactions and shell model calculations are consistent with each other.

If the spectroscopic factors are known from shell model calculations, it is determined that how far the reaction coefficient R in Eq. (1) is from the ideal value of 1:

$$R = d\sigma/d\Omega)_{exp}/d\sigma/d\Omega)_{DWBA} \cdot (S_{ab}S_{AB})_{shell\ model} \qquad (3)$$

A reaction coefficient of $R \sim 7$ is obtained for the ^{58}Ni(^{16}O, ^{12}C$_{g.s.}$)^{62}Zn$_{g.s.}$ transition at the 80 MeV incident energy.

5-3. Angular distribution of the g'nd 0^+ state.

The angular distribution shape of the g'nd 0^+ transition changes with the incident energy as shown in fig. 11. Data at 46 and 60 MeV incident energies are taken from data of Berg *et al.*[8,36] Data points for the 46 MeV incident energy show a typical bell shape angular distribution. Those for the 60 MeV incident energy reveal a forward peaked and pronounced oscillation pattern in the whole angular region. Those for the 80 MeV incident energy show the oscillations damping with the reaction angle and then a monotonous fall at larger angles.

Solid curves in Fig. 11 represent the results of the EFR-DWBA calculations with the same OM parameter set I as in the case of the 80 MeV incident energy. The dependence of the angular distribution shape on the incident energy is roughly reproduced with only one OM parameter set over the wide incident energy range.

Absolute spectrosopic factors $R \cdot S_{ab}S_{AB}$ determined from Eqs. (1) and (3) are listed in Table III for the present 80 MeV, 46 and 60 MeV data.[36] The OM parameters A and B in Table III correspond to the OM parameters set I-C and II in Table I, respectively.

5-4. Spins of the energy levels in ^{62}Zn

Energy levels populated by the ^{58}Ni(^{16}O, ^{12}C)^{62}Zn reaction are listed in Table 2. The spin-parties were adopted from comparison with other scattering and reaction measurements,[21] and then assumed in the EFR-DWBA calculations.

The g'nd and 0.95 MeV l'st excited states have the assignments of 0^+ and 2^+, respectively. The 1.81 MeV state has the assignment of 2^+ in (^{6}Li, d)[10,27] and (p, t)[31]

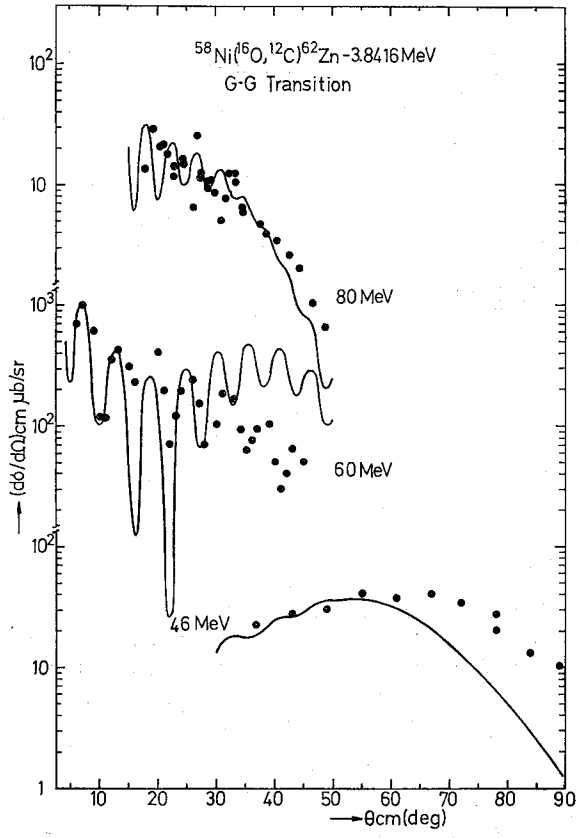

Fig. 11. Cross section angular distributions of the ^{58}Ni (^{16}O, ^{12}C) ^{62}Zn reaction leading to the g'nd 0^+ transition at 46, 60 and 80 MeV incident energies. Data at 46 and 60 MeV incident energies were taken from Ref. 8. Curves show the EFR-DWBA calculations described in the text.

Table III, The factor $R \cdot S_{ab}S_{AB}$, reaction coefficient R, and the ratio of the factor $R \cdot S_{ab}S_{AB}/(R \cdot S_{ab}S_{AB})_{80}$. Symbols A and B indicate the OM parameters I-c and II in Table, 1, respectively.

OM darameter	A			B		
E_{1ab} (^{16}O) (MeV)	$RS_{ab}S_{AB}$	R	$\frac{RS_{ab}S_{AB}}{(RS_{ab}S_{AB})_{80}}$*	$RS_{ab}S_{AB}$	R	$\frac{RS_{ab}S_{AB}}{(RS_{ab}S_{AB})_{80}}$
80	2×10^{-2}	~ 7	1	2×10^{-2}	~ 7	1
60	3×10^{-1}	100	15.4	1.5×10^{-2}	5	0.75
46	8.3×10^{-3}	~ 3	0.42	8.5×10^{-3}	~ 3	0.43

*; Comparison with the value at 80 MeV, **; Ref. 36

reactions. The 2.19 MeV state has the assignment of 4^+ in the same reactions as the 1.81 MeV state. The 2.33 MeV state has the assignment of 0^+ in (^6Li, d)[10,27], (τ, n)[30] and (p, t)[31] reactions. The 2.74 and 2.80 MeV states have presumably the assignments of 4^+ and 2^+, respectively. However, the spins and parities of these levels have not been

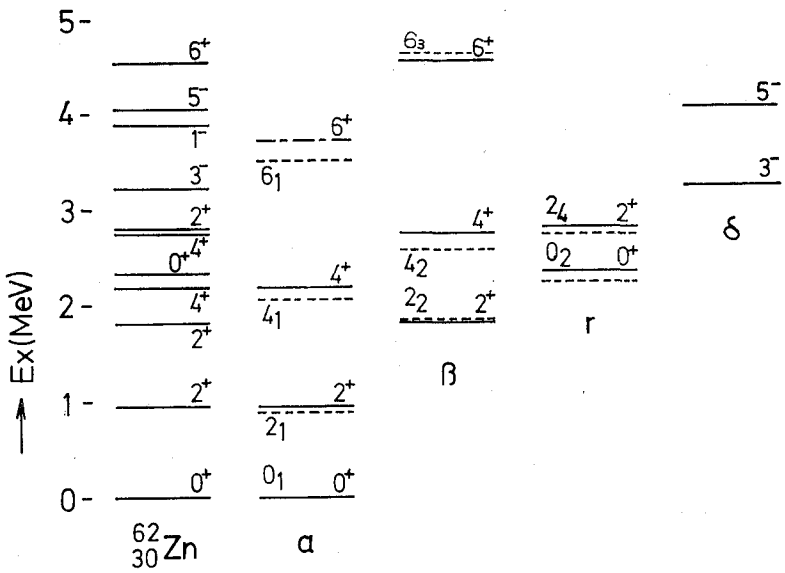

Fig. 12. Classification of the energy levels in the framework of collective model. Solid and dotted lines represent the experimental and theoretical energy levels described in the text, respectively.

assigned in the (^{6}Li, d) reactions.[27,28] The 3.22 MeV state has the assignment of 3$^-$ with two exceptions (4$^+$ or 3$^-$[28] in the (^{6}Li, d), and 2$^+$ or 3$^-$[30] in the (τ, n) reactions.) The 3.88 MeV state has the assignment of 1$^-$.

The energy levels of ^{62}Zn discussed above are classified in four groups α, β, γ and δ, in the framework of collective model as shown in Fig. 12. The l'st 6$^+$ excited state has been observed at the excitation energy of 3.71 MeV by the in-beam γ spectroscopies[39,40,41]. However, this state has no evidence for the population in the transfer data as shown in Fig. 9. The α level group corresponds to the g'nd band observed in the in-beam γ spectroscopies[39,40,41]. The other level groups correspond to side-bands in the phonon and rotational nuclear model[10] or in the cluster-vibration model[42]. The shell model predictions of Bennett *et al.*[33] are given by dotted lines for comparisons in Fig. 12.

5-5. Continuum state

The data in Fig. 4 is a typical energy spectrum of the ^{58}Ni(^{16}O, ^{12}C)^{62}Zn reaction leading to the continuum state. These energy spectra exhibited broad bell shaped distributions peaked at the excitation energy of around 16 MeV. The data in Fig. 7 correspond to the angular distribution of the ^{12}C total yields integrated over the energy on the continuum energy spectra. The distribution decreases smoothly with the angle as seen in Fig. 7. The characteristics of the results in this experiment are in agreement with other experiments.[43,44] The ^{58}Ni(^{16}O, ^{12}C) contimuum spectra have been measured at three incident energies, 64, 72 and 81 MeV.[43] The angular and energy dependences of the optimum Q value have been deduced from the data and discussed by combining the recoil model with a concept of nuclear friction. An attempt was made to fit the

angular distribution based on the DWBA formalism using the diffraction model.[44] The continuum state may by explained by the previous formalism used for discrete transitions given in sect. 4-2 with some simplifications. A main difficulty in such calculations for the population of these states is lack of the knowledge connected with the level density of the residual nucleus.

§ 6. SUMMARY

The cross section angular distributions for the $^{16}O+^{58}Ni$ elastic scattering and the $^{58}Ni(^{16}O, ^{12}C)^{62}Zn$-3.8416 MeV reaction were measured at the incident energy E_{lab} (^{16}O) =80 MeV. The optical model parameters were deduced from the best fit to the data of the $^{16}O+^{58}Ni$ elastic scattering. The EFR-DWBA calculations were performed for the angular distributions of the $^{58}Ni(^{16}O, ^{12}C)^{62}Zn$ reaction. The results are summarized as follows:

(1) Some discrete levels were observed in the energy spectra of the $^{58}Ni(^{16}O, ^{12}C)^{62}Zn$ reaction with the cross section of 1~200 μb/sr. The selectivity of the (^{16}O, ^{12}C) reaction is similar to that of the (^{6}Li, d) reaction.

(2) The (^{16}O, ^{12}C) reaction was enhanced in the particle identification spectra of the ^{16}O induced reactions on ^{58}Ni. This is because the Q value of this reaction is negative but small.

(3) The ground-state cross-section was found to change with incident energy by comparing the present data with the other data at 46 and 60 MeV.

(4) The shape of the angular distribution for the g'nd state transition changes with the incident energy. The 46 MeV angular distribution shows typical bell shape. The 60 MeV angular distribution reveals the forward peaked and pronounced oscillation pattern. The 80 MeV angular distribution displays the oscillations damping with the angle and the monotonous fall on the angle.

(5) The EFR-DWBA calculations reproduce the gross features of the angular distributions.

(6) The OM parameters giving good representation of the data have the property that the real diffuseness parameter has a large value.

(7) The inclusion of Coulomb correction in the transfer interaction causes a reduction of 0.9 times in cross section, but no change in angular distribution.

(8) The dependence of the angular distribution shape on the incident energy is reproduced by the EFR-DWBA calculation even if only one OM parameters set is used over the wide incident energy range.

(9) Deduced relative spectroscopic factors are consistent with results of the other experiments and shell model predictions.

(10) The reaction coefficients deduced at different incident energies are consistent with each other.

ACKONWLEDGEMENT

The authors would like to thank Dr. J. Schimizu of University of Tsukuba and

Mr. T. Shiba of Mitsubishi Electric Corporation for their interests and helps throughout the measurements.

REFERENCES

(1) D. Kurath, *Phys. Rev.*, **C7**, 1390 (1973).
(2) K. Bethge, *Ann. Rev. Nucl. Sci.*, **20**, 255 (1970).
(3) J. R. Erskine, W. Henning, and L. R. Greenwood, *Phys. Lett.*, **47B**, 335 (1973).
(4) D. L. Hanson, N. Stein, J. W. Sunier and C. W. Woods, *Phys. Rev. Lett.*, **38**, 587 (1977) : *Nucl. Phys.*, **A321**, 471 (1979).
(5) R. M. DeVries, *Phys. Rev. Lett.*, **30**, 666 (1973).
(6) R. M. DeVries, D. Shapira, W. G. Davies, G. C. Ball, J. S. Forste and W. McLatchie, *Phys. Rev. Lett*, **35**, 835 (1975).
(7) W. G. Davies, R. M. DeVries, G. C. Ball, J. S. Forster, W. McLatchie, D. Shapira, J. Toke and R. E. Warner, *Nucl. Phys.*, **A269**, 477 (1976).
(8) G. P. A. Berg, B. Berthier, J. P. Fouan, J. Gastebois, J. P. Le Févre and M.-C. Lemaire, *Phys. Rev.*, **C18**, 2204 (1978).
(9) G. Delic, K. Pruess, L. A. Charlton and N. K. Glendenning, *Phys. Lett.*, **69B**, 20 (1977).
(10) M. Sakai, *Pro. Inter. Conf. on Nuclear Structure, Tokyo*, p. 576 (1976).
(11) T. Marumori, M. Yamamura, Y. Shono, A. Tokunaga and Y. Miyanishi, *Proc. Inter. Conf. on Nuclear Structure*, Tokyo, p. 581 (1967).
(12) H. Faraggi, M.-C Lemaire, J.-M. Loiseaux, M. C. Mermaz and A. Papineau, *Phys. Rev.*, **C4**, 1375 (1971).
(13) H. Faraggi, A. Jaffrin, M.-C. Lemaire, M. C. Mermaz, J.-C. Faivre, J. Gastebois, B. G. Harvey, J.-M. Loiseaux and A. Papineau, *Ann. Phys.* (N. Y.), **66**, 905 (1971).
(14) M. -C. Lemaire, *Phys. Report*, **7C**, 279 (1973).
(15) R. A. Brogia and P. F. Bortignon, *Phys. Lett*, **64B**, 259 (1976).
(16) R. R. Betts, *Phys. Rev.*, **C16**, 1617 (1977).
(17) R. A. Broglia, L. Ferreira, P. D. Kunz, H. Sofia and A. Vitturi, *Phys. Lett.*, **79B**, 351 (1978).
(18) Y. Ōkuma, T. Yanabu, S. Matsuki, T. Motobayashi, K. Takimoto, T. Shimoura, K. Ogino and M. Fukada, *Spring Metting of Phys. Soc. Japan, Hiroshima*, (1981).
(19) Y. Ōkuma, T. Yanabu, S. Matsuki, T. Motobayashi K. Takimoto, T. Shimoura, K. Ogino, M. Fukada and J. Shimizu, *RCNP Annual Report 1981*, p. 93 (1981).
(20) Y. Ōkuma, T. Yanabu, S. Matsuki, T. Motobayashi, K. Takimoto, T. Shimoura, K. Ogino and M. Fukada, *RCNP Annual Report 1981*, p. 102 (1981).
(21) *"Table of Isotopes,"* 7th edition, edited by C. M. Lederer and V. S. Shirley, John Wiley & Sons, Inc. (1978).
(22) M. S. Zisman, R. M. DeVr es, J. G. Cramer, K. L. Liu, Y. D. Chan, and B. Cuengco, *Phys. Rev.*, **C11**, 809 (1975).
(23) R. M. DeVries, private communications.
(24) T. A. Brody and M. Moshinsky, "Table of Transformation Brackets for Nuclear Shell Model Calculations", (Gordon and Breach, N. Y., 1967).
(25) R. M. DeVries, *Phys. Rev.*, **C11**, 2195 (1975).
(26) E. Mathiak, K. A. Eberhard, J. C. Cramer, H. H. Rossner, J. Stettmerier, and A. Weidinger, *Nucl. Phys.*, **A259**, 129 (1976).
(27) H. W. Fulbright, C. L. Bennett, R. A. Lindgren, R. G. Markham, S. C. McGuire, G. C. Morrison, V. Strohbush and J. Tōke, *Nucl. Phys.*, **A284**, 329 (1977).
(28) H. H. Gutbrod and R. G. Markham, *Phys. Rev. Lett.*, **29**, 808 (1972).
(29) M. B. Greenfield and C. R. Bringham, *Phys. Rev.*, **C6**, 1756 (1972).
(30) D. Evers, W. Assmann, K. Pudolph and S. J. Skorka, *Nucl. Phys.*, **A230**, 109 (1974).
(31) R. A. Hinrichs and D. M. Patterson, *Phys. Rev.*, **C10**, 1381 (1974).
(32) J. C. Peng, J. V. Maher, W. Oelert, D. A. Sink, C. M. Cheng and H. S. Song, *Nucl. Phys.*, **A264**, 312 (1976).

(33) C. L. Bennett, H. W. Fulbright, J. F. A. van Hienen, W. Chung and B. H. Wildenthal, *Phys. Rev.*, **C19**, 1099 (1979).
(34) G. R. Satchler, *Nucl. Phys.*, **A379**, 493 (1977).
(35) P. J. Moffa, C. B. Dover and J. P. Vary, *Phys. Rev.*, **C23**, 147 (1976).
(36) M. C. Mallet-Lemaire, *AIP Conf. Pro. No.* 47., "Clustering Aspects of Nuclear Structure and Nuclear Reactions,", editors W. T. H. Vox Oers, J. P. Svenne, J. S. C. Mckes and W. R. Falk, Winnipeg, p. 271 (1978).
(37) C. L. Bennett, *Nucl. Phys.*, **A284**, 301 (1977).
(38) L. West, Jr., K. W. Kemper and N. R. Fletcher, *Phys. Rev.*, **C11**, 859 (1975).
(39) L. Mulligan, R. M. Aurmuble and D. P. Baramuth, *Bull. Amer. Phys. Soc.*, **23**, 573, GF3 (1978).
(40) J. F. Bruandet, Tsan Ung Chan, M. Agard, J. P. Longequeue, C. Morand and A. Giorni, *S. Phys.*, **A279**, 69 (1976).
(41) H. Kusakari, T. Suehiro, M. Ishihara, M. Kawakami, N. Yoshikawa and M. Saeki, *J. Phys. Soc. Japan*, **34**, 865 (1973).
(42) V Lopac and V. Paar, *Nucl. Phys.*, **A297**, 471 (1978).
(43) J. Wilczynski, K. Siwek-Wilczynska, J. S. Larsen, J. C. Acquadro and P. R. Christenssn, *Nucl. Phys.*, **A244**, 147 (1975).
(44) M. C. Mermaz, *Phys. Rev.*, **C21**, 2356 (1980).
(45) R. R. Betts, Nelson Stein, J. W. Sunier and C. W. Woods, *Phys. Lett.*, **76B**, 47 (1978).